Lattice distortion in $In_xGa_{1-x}As/InP$ epitaxial films: A second- and third-shell XAFS study

M. Tormen,* D. De Salvador, and A. V. Drigo
Istituto Nazionale Fisica della Materia (INFM), c/o Dipartimento di Fisica ''G.Galilei'' via Marzolo 8, I-35131 Padova, Italy

F. Romanato
TASC-INFM at Elettra Synchrotron SS.14 Km 163.5 I-32 Basovizza, Trieste, Italy

F. Boscherini
Istituto Nazionale per la Fisica della Materia and Dipartimento di Fisica, Universitá di Bologna, viale C. Berti Pichat 6/2, 40127 Bologna, Italy

S. Mobilio
INFN, Laboratori Nazionali di Frascati, P.O. Box 13, I-00044 Frascati, Italy and Dipartimento di Fisica, Universita Roma Tre, Via della Vasca Navale 84, 00146 Roma, Italy

(Received 15 May 2000; revised manuscript received 20 September 2000; published 2 March 2001)

We investigate the lattice distortion of pseudomorphic epitaxial $In_xGa_{1-x}As/InP$ thin films by polarization-dependent x-ray absorption fine-structure spectroscopy; five samples with In concentration in the range 0.25–0.75 and strain ranging from tensile to compressive have been investigated. We find that the measured second- and third-shell distances exhibit a clear dependence on the angle between the photon beam and the sample normal, in agreement with the expected tetragonal distortion of the unit cell. A method is proposed to extract from the polarization-dependent measurements the values of the strain-induced split of second- and third-shell interatomic distances. The values obtained by this method are in excellent agreement with the predictions of a model that calculates the variations of interatomic distances due to strain by applying the macroscopic strain tensor at local scale and linearly summing the known alloying effect. This model was applied successfully to the first shell distances in previous papers; the application to the second and third shells is a further confirmation of the validity of the model in the $In_xGa_{1-x}As$ structure.

DOI: 10.1103/PhysRevB.63.115326 PACS number(s): 68.60.Bs, 61.10.Ht, 61.66.Dk, 62.20.Dc

I. INTRODUCTION

Although x-ray diffraction has demonstrated that III-V and II-VI pseudobinary semiconductor alloys have the same long-range order as exhibited by binary alloys, x-ray absorption fine structure spectroscopy[1,2] (XAFS) has highlighted significant local deviations from the undistorted zinc-blende atomic arrangement. Since this discovery, the characterization and the understanding of the local distortion in semiconductor alloys has much advanced,[3–5] and now there is a wide consensus concerning this behavior of bulk alloys. The static disorder in the lattice has been ascribed to the presence of different covalent bond lengths in the alloys (alloying disorder).

In recent last years, however, the interest has turned towards the comprehension of short-range order in systems of semiconductor alloys with strain. Indeed this is an important issue for a better understanding of the actual atomic arrangement in low-dimensional systems, where high values of epitaxial strain can be reached. Furthermore, strain represents an additional parameter that can be exploited to study the accommodation of bond-length misfit.

Bond-length variations in strained semiconductor thin epitaxial films have been investigated in a series of XAFS studies.[6–9] In earlier papers,[10,11] we have demonstrated that nearest-neighbor (NN) interatomic distances in strained film can be evaluated by applying the matrix of macroscopic strain down to the interatomic scale and linearly summing this effect to that due to alloying. However, the available data for the influence of the external strain field on the first-neighbor distances are not sufficient to completely determine the cell distortion. We have extended our investigation up to the second and third coordination shells, by performing polarization-dependent XAFS measurements on the same set of $In_xGa_{1-x}As/InP$ pseudomorphic epitaxial films studied in Ref. 10.

Tensile, compressive, and lattice-matched (corresponding to the composition $x=0.532$) epilayers grown on [001] InP substrates have been analyzed by fluorescence-detected XAFS. In Ref. 10 we demonstrate that our measurements are sensitive enough to detect the length variation suffered by Ga-As and In-As atomic bonds under epitaxial strain. In the present paper, we will show that the second and third coordination shells undergo a complex strain-induced deformation that introduces a supplementary splitting in the distribution of distances, which is already split by the alloying effect.[1]

Indeed, since the unit cell of epitaxial layers is tetragonally distorted, it is natural to expect that the interatomic distances oriented close to the surface normal are increased and those close to the surface plane are contracted in the case of compressive strain. The opposite will happen in the case of tensile strain. We exploit the polarization sensitivity of XAFS (Ref. 12) in order to detect this effect. The experimental data are reproduced by our model (Refs. 10 and 11) based on the application of the strain deformation matrix down to the interatomic distance scale.

TABLE I. Structural parameters of the investigated samples: Indium atomic fraction x, parallel strain $\epsilon_{\parallel}$, layer thickness.

Sample	x (at. %)	$\varepsilon_{\parallel}$ (%)	Thickness (nm)
A	25.0	1.95	26
B	31.6	1.60	80
C	52.4	0.06	460
D	70.5	−1.18	30
E	75.7	−1.42	8

II. EXPERIMENT

Five $In_xGa_{1-x}As$ epitaxial films have been grown by metal-organic vapor phase epitaxy on InP [001] substrates at a temperature of 650 °C (Ref. 10) with composition ranging between 25 and 75 at. % (see Table I).

Complementary structural characterization has been performed by high resolution x-ray diffraction (HRXRD) and Rutherford backscattering spectrometry (RBS) in order to determine the strain matrix and the sample composition and thickness. HRXRD measurements were performed with a Philips MRD high resolution diffractometer following standard procedures[13] collecting ω-2θ scans of the 004 and 444 reflections at the four azimuths along the $\langle 110 \rangle$ in-plane directions. RBS-channeling measurements were performed using a 2-MeV ^{4}He beam delivered by the AN-2000 Van de Graaff accelerator of the National Laboratories of Legnaro (Italy).[14]

XAFS measurements were performed at the European synchrotron radiation facility in Grenoble (France) at the GILDA beamline, using a dynamically, sagitally focusing Si(311) monochromator;[15] higher harmonics were rejected by a pair of grazing incidence, Pd-coated mirrors. The measurements were performed at 77 K in order to reduce the thermal vibration. The spot size was approximately 1×2 mm^2 and the photon flux approximately 5×10^{10} photons per second. Fluorescence detection was performed with a seven-element hyperpure Ge detector collecting spectra at the Ga (10 150–11 700 eV energy range) and As (11 700–13 000 eV) *K* edges; the shaping time of the amplifiers was 0.25 μs and the total count rate on each detector element was kept below 30 000 counts/s to avoid nonlinearity problems. The integration time was chosen in order to keep signal-to-noise ratio equal to 1000.

Fluorescence XAFS spectra on single crystals may be distorted by two kinds of effects. The first is the presence of intense Bragg peaks that directly hit one or more of the seven detector elements, thus saturating them; this effect is eliminated by excluding the saturated elements from consideration. The second, more subtle, effect is due to the excitation of x-ray standing waves in narrow energy regions giving rise to modulations of the fluorescence intensity; this spurious effect has been eliminated by using a vibrating sample holder that continuously changes the Bragg condition during data collection, thus completely smoothing-out the spurious peaks.[11]

Each spectrum has been collected at least twice using different sample orientations with respect to the x-ray polarization. In one case, the x-ray polarization was nearly parallel to the films surface (the polarization direction was at an angle $\xi=75°$ from the normal to the surface). In the other case, the polarization was nearly normal to the surface ($\xi=20°$). This kind of experimental setup is chosen in order to detect the anisotropic distribution of distances of the strained sample.[12]

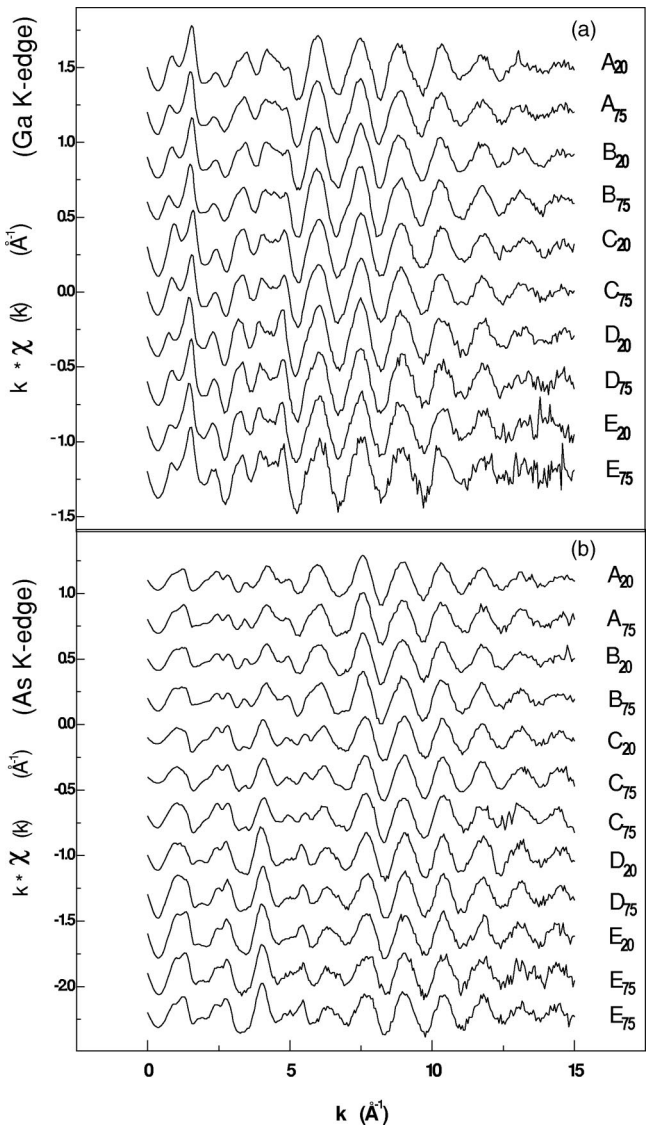

FIG. 1. XAFS oscillations extracted from the x-ray absorption measurements at the Ga *K* edge (a) and at the As *K* edge (b). The measured samples (*A*, *B*, *C*, *D*, and *E*) are sorted by increasing In content. The numerical index 20 or 75 represents the angle, in degrees, between the polarization of the photon beam and the normal to the epitaxial film.

III. XAFS DATA ANALYSIS

Data analysis was performed by an *ab initio* modeling of the signal using the FEFF code,[16] and a least square fitting of the experimental XAFS signal (FEFFIT code).[17] The latter is extracted from the absorption spectrum using the AUTOBK code[18] (provided in the FEFF package). The absorption back-

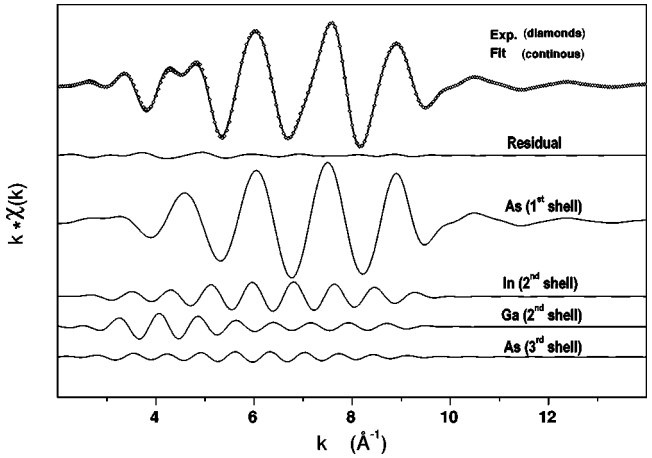

FIG. 2. Filtered Fourier-backtransformed fit of a XAFS signal relative to the sample *B*, In content $x=31.6$ at. %, collected at the Ga *K* edge with the angle between the polarization vector and the sample normal $\xi=20°$.

ground was obtained by selecting a linear fit of the pre-edge region in the interval -200 to -50 eV below the edge (10 363 eV for Ga and 11 867 eV for As) and by fitting the spectrum above the edge with a cubic spline forcing the Fourier transform of the XAFS to be null below the radial distance of 1.0 Å. The extracted XAFS signals at the Ga and As *K* edge are plotted versus the photoelectron wave vector *k* in Fig. 1. The high quality of the data is apparent.

The signals were Fourier transformed into *r*-space (using a Hanning window with edge-smoothing parameter $\Delta k=0.5$ Å^{-1}) in the interval $[k_{min},k_{max}]$ and using a weighting function k^w. The *k* range and the weight *w* were [3,9] Å^{-1} and 1.5 for the Ga edge and [4,12] Å^{-1} and 1.0 for the As edge.

As well known, statistical experimental noise is transformed into white noise when the Fourier transform of the signal is performed.[17] This noise level generally decreases when the *k* range $(k_{max}-k_{min})$ and the value of *w* are reduced. On the other hand, high *w* values allow to minimize systematic errors originating from not perfect background subtraction and errors in modeling and a large *k* range usually brings a greater amount of structural information. In our previous work (Ref. 11), a value of $w=2$ and a *k* range of 13 Å^{-1} were adopted for first-shell analysis. However, such choice is not optimal for the analysis of the second and third coordination shells. This fact can be ascertained by looking, for instance, at the errors on the fitting parameters estimated by the fit for different values of *w* and k_{max}. As a rule, the choice that allows to minimize the errors depends on whether the fitting parameters considered are those relative to the first or to the higher coordination shells. As reported, the values of *w* and k_{max} here adopted for the analysis of the second- and third-shell analysis are smaller than those used previously for the first shell. This reflects the smaller *k*-space extent of the signal components of the higher coordination shells with respect to that of the first shell.

The theoretical signals were calculated for a model cluster containing atoms of In, Ga, and As up to the fifth coordination shell around the photo-absorber (Ga or As). An equal number of In and Ga atoms was distributed in the cationic sublattice and their location was chosen in such a way that all the possible two- and three-body arrangements up to a cut-off path length $2R=12$ Å, were represented in the model cluster. The virtual crystal approximation was adopted as the structural model for the cluster, and the corresponding lattice parameter chosen for the calculation of the XAFS signals was set equal to that of $In_{0.5}Ga_{0.5}As$ ($a_{cluster}=5.8558$ Å). The fitting procedure on the experimental spectra was performed by means of FEFFIT code, that allows to correct the theoretically generated signals according to the change of the structural parameters. Fitting was performed in *R* space in the interval [1.7,4.9] Å, on the signal obtained by Fourier transform in the ranges $[k_{min},k_{max}]$ described above.

The structural parameters used in the fit of Ga edge spectra are the first-shell distance $r^{1st}_{\text{Ga-As}}$ with the corresponding Debye-Waller factor $\sigma^{1st}_{\text{Ga-As}}$, two distances for the second shell, $r^{2nd}_{\text{Ga-Ga}}$ and $r^{2nd}_{\text{Ga-In}}$, with a common Debye Waller factor $\sigma^{2nd}_{\text{Ga-(Ga/In)}}$, and a third shell distance $r^{3rd}_{\text{Ga-As}}$ with the relative

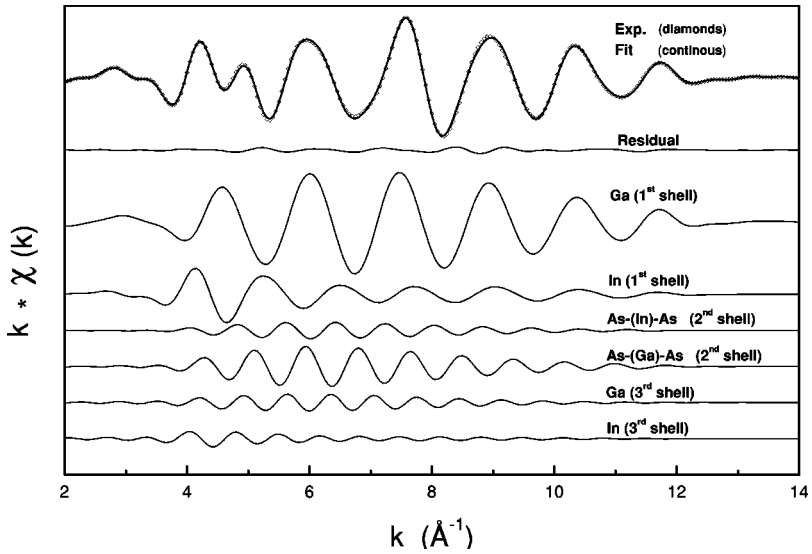

FIG. 3. Filtered Fourier-backtransformed fit of a XAFS signal relative to the sample *B*, In content $x=31.6$ at. %, collected at the As *K* edge with the angle between the polarization vector and the sample normal $\xi=20°$.

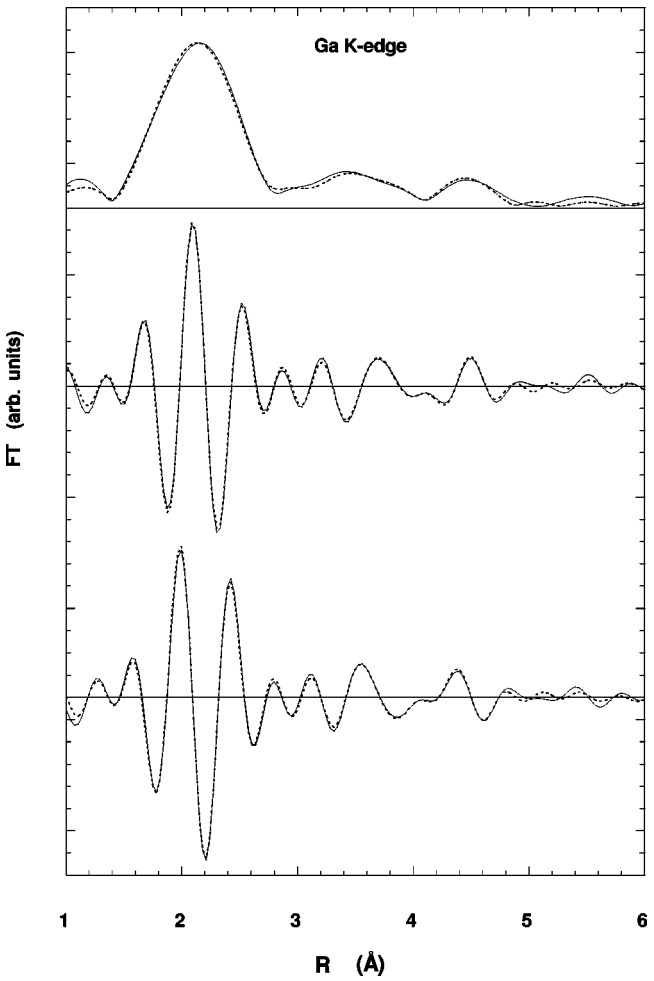

FIG. 4. *r*-space plot of the filtered spectra shown in Fig. 2. From top to bottom, amplitude, real and imaginary part of the experimental spectra (continuous line) and of the fit (dashed line).

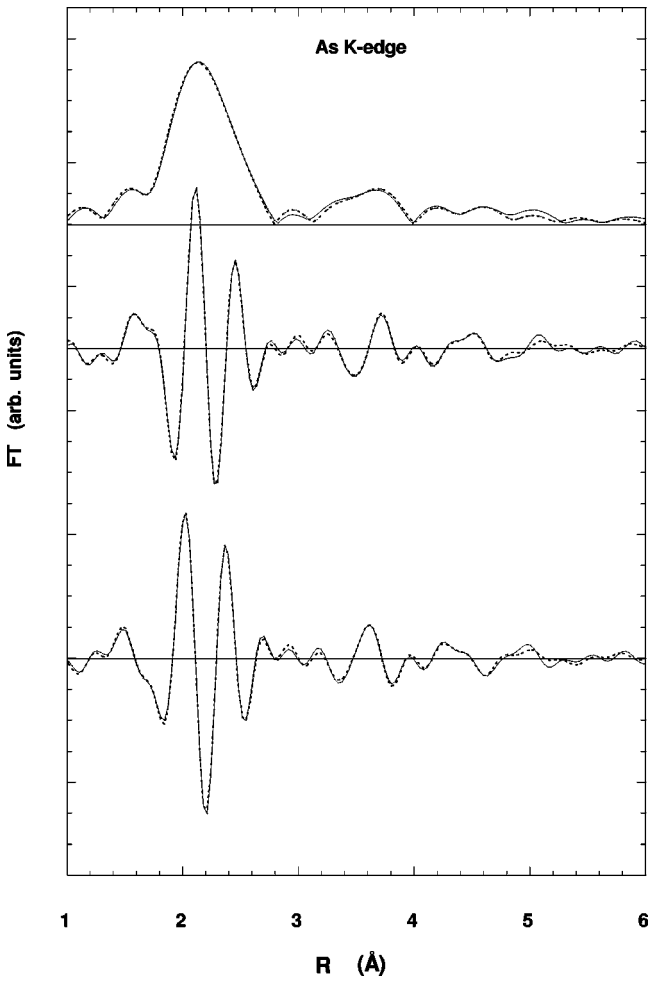

FIG. 5. *r*-space plot of the filtered spectra shown in Fig. 3. From top to bottom, amplitude, real and imaginary part of the experimental spectra (continuous line) and of the fit (dashed line).

Debye-Waller factor $\sigma^{3rd}_{\text{Ga-As}}$. In order to reproduce the As-edge spectra, the following structural parameters are used: two first shell distances, $r^{1st}_{\text{As-Ga}}$ and $r^{1st}_{\text{As-In}}$, two second shell distances, $r^{2nd}_{\text{As-(In)-As}}$ and $r^{2nd}_{\text{As-(Ga)-As}}$, and a single third shell distance $r^{3rd}_{\text{As-(Ga/In)}}$. The last value is used in order to generate both the third shell As-In and As-Ga signals. In the case of the As edge a single Debye-Waller factor for each shell is used ($\sigma^{1st}_{\text{As-(Ga/In)}}$, $\sigma^{2nd}_{\text{As-As}}$ and $\sigma^{3rd}_{\text{As-(Ga/In)}}$). Besides the described structural parameters the usual XAFS free parameters E_0 (edge energy) and S_0^2 (many-body amplitude reduction factor) are optimized in the fit. Total coordination numbers were always fixed to their crystallographic value. In the fit the most important multiple scattering (MS) signals were also included. Finally, the error bars on the fitting parameters are those determined by FEFFIT, i.e., the square root of the diagonal elements of the correlation matrix. The procedure used by FEFFIT to estimate the error bars is consistent with the criteria adopted by the International XAFS Society.[19]

In Figs. 2 and 3 we compare the filtered contributions from the first three coordination shells with the fit. Also shown are the residual and the separate signals used in the fitting; the excellent quality of the fit is apparent. Though the fit is limited to the interval $k \in [k_{min}, k_{max}]$, the XAFS signal is well reproduced up to $k = 17.0$ Å^{-1}, indicating that the component relative to the first shell is reliably taken into account although the interval was selected specifically to extract the contribution of second and third shells. The values obtained for the first shell distances are in agreement with those already published.[10] The MS signal, included in the fit procedure, is not shown because of its relative weakness.

Figures 4 and 5 show the comparison of the Fourier transforms (magnitude, imaginary and real part) of the data and of the fit corresponding to the signals of Figs. 2 and 3. It is clear also from this figure that all spectral features in the *R*-space interval of interest are reproduced very well by the fit.

IV. RESULTS

XRD and RBS-channeling structural characterization has shown that the epitaxial layers are pseudomorphic, i.e., their thickness is below the critical value for the beginning of the epitaxial strain relaxation (see Table I). The reported errors correspond to one standard deviation. The cross check of In atomic measurement performed by RBS and by XRD has

TABLE II. Second and third shell distances from XAFS measurements at the As and Ga *k* edges and at two different orientations of the polarization vector. Columns 1,2: sample code, angle ξ (degrees) between the normal to the film and the polarization vector. Columns 3–5: second-shell distances of the type $r_{\text{As-(Ga)-As}}$ and $r_{\text{As-(In)-As}}$, and common value of third-shell distances of types $r_{\text{As---Ga}}$, $r_{\text{As---In}}$, obtained from spectra at the As *k* edge. Columns 6–8: second shell distances $r_{\text{Ga-(As)-Ga}}$ and $r_{\text{Ga-(As)-In}}$, and third shell distance $r_{\text{Ga---As}}$, measured at the Ga *k* edge.

		As *k*-edge			Ga *k* edge		
sample	ξ (deg)	$r_{\text{As-(Ga)-As}}$ (Å)	$r_{\text{As-(In)-As}}$ (Å)	$r_{\text{As---(Ga/In)}}$ (Å)	$r_{\text{Ga-(As)-Ga}}$ (Å)	$r_{\text{Ga-(As)-In}}$ (Å)	$r_{\text{Ga---As}}$ (Å)
A	20	4.043±0.007	4.240±0.025	4.841±0.014	4.079±0.006	4.129±0.016	4.762±0.029
	75	4.076±0.009	4.308±0.034	4.898±0.014	4.128±0.011	4.175±0.010	4.873±0.025
B	20	4.049±0.006	4.262±0.016	4.849±0.012	4.098±0.005	4.137±0.012	4.796±0.025
	75	4.076±0.012	4.299±0.033	4.890±0.015	4.123±0.010	4.167±0.009	4.869±0.021
C	20	4.064±0.014	4.303±0.014	4.910±0.014	4.147±0.012	4.200±0.014	4.909±0.034
	75	4.049±0.029	4.315±0.034	4.874±0.026	4.137±0.013	4.194±0.006	4.899±0.029
D	20	4.045±0.045	4.314±0.017	4.946±0.019	4.172±0.019	4.232±0.013	4.963±0.041
	75	3.995±0.069	4.305±0.030	4.897±0.025	4.183±0.039	4.211±0.008	4.924±0.036
	75				4.153±0.035	4.208±0.009	4.900±0.040
	75				4.171±0.041	4.207±0.009	4.929±0.042
E	20	4.032±0.061	4.319±0.020	4.932± 0.031	4.143±0.035	4.227±0.016	4.931±0.062
	75	4.003±0.075	4.305±0.024	4.892± 0.023	4.133±0.062	4.215±0.011	4.896±0.047
	75	3.966±0.094	4.301±0.032	4.887±0.020	4.168±0.064	4.219±0.010	4.960±0.059

shown the absence of any systematic deviation. These results validate the linear dependence of the mean lattice constant (Vegard's law) within an error bar of ±0.02 Å. The lattice tetragonal distortion of all the epilayers have been measured and the values of the parallel strain have been reported in Table I. It results that the epilayer strain changes from tensile to compressive as a function of In content. Moreover AFM investigations of tensile samples have shown that the surface is free from cracks and atomically flat.

The results of the XAFS data analysis relative to the second and the third shell distances are reported in Table II. The reported errors correspond to one standard deviation. In Figs. 6–9, the values of the different distances are shown as a function of the In concentration together with their linear fits relative to both the used polarization orientations. From the linear fits it appears that the two polarization orientations do not give the same results except around the composition $x = 50$ at. % where the strain is nearly null. In the case of tensile strain ($x < 53$ at. %) the distances measured for $\xi = 75°$ are greater than those measured for $\xi = 20°$. The opposite occurs for compressive strain ($x > 53$ at. %). The slope of the fit increases for the data collected with the polarization vector almost perpendicular to the sample surface ($\xi = 20°$).

V. POLARIZATION DEPENDENCE IN STRAINED LAYERS

The different composition dependence of the data relative to the two polarizations can be understood as a consequence of the symmetry reduction of the unit cell, from cubic to tetragonal.

When the crystal is tetragonally distorted, the second and third shell sites are split in two subsets of equivalent sites. Considering for instance a compressive strain, we expect that the length of the vector connecting the photoabsorber to an arbitrary atom $\vec{r}$ is increased if oriented along the normal to the growth plane. The contrary will happen for vectors $\vec{r}$ parallel to the growth plane. In general, in tetragonal strained samples, the lengthening or shortening of interatomic distances depends essentially on the angle between the plane (001) and the vector $\vec{r}$.

Based on the previous reasoning, we do not expect any distance splitting for the atoms of the first shell. In fact all the vectors $\vec{r}$ relative to the 4 NN form the same angle respect to the normal to the plane (001). On the contrary, the atoms of the second shell can be divided into two subsets. Four atoms lie *in* the (001) plane at distance $r_{2nd}^{(in)}$ (see Fig. 10). The other eight atoms lie *out* of the (001) plane, at distance $r_{2nd}^{(out)}$, with the vector $\vec{r}$ that forms an angle of 45° with the (001) plane. It results that each of the second shell distances obtained from the fit procedure, i.e., Ga-Ga, Ga-In, As-(Ga)-As, As-(In)-As, is split in two subsets of interatomic distances (*in* and *out*). A similar split occurs also for the 12 atoms of the third shell: there are eight atoms at distance $r_{3rd}^{(in)}$ whose position vector form an angle of 17.55° with the plane and four at distance $r_{3rd}^{(out)}$ forming an angle of 64.76°.

Various attempts to fit independently the two subsets in which each of the second- and third-shell distances are split have been done. The convergence procedure failed systematically due to the presence of too many correlated parameters. Consequently, in the following we describe a different procedure that exploits the XAFS polarization dependence.

It is known that XAFS signal of a single scattering atom is weighted by the factor $3\cos^2(\theta)$ (Refs. 20–22), where θ

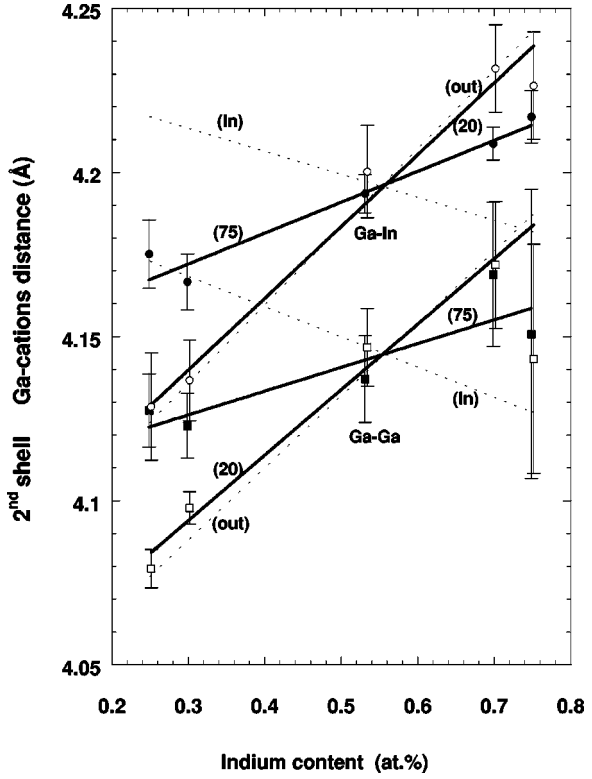

FIG. 6. Ga-cations second shell distances versus In atomic fraction: squares refer to $r^{2nd}_{\text{Ga-Ga}}$, circles to $r^{2nd}_{\text{Ga-In}}$. Solid and open symbols indicate respectively measurement collected at two polarization incidence angle: $\xi=75°$ and $\xi=20°$. Linear fits of the different data set are represented by continuous lines. Dashed lines show the linear dependence calculated for *in* and *out* components.

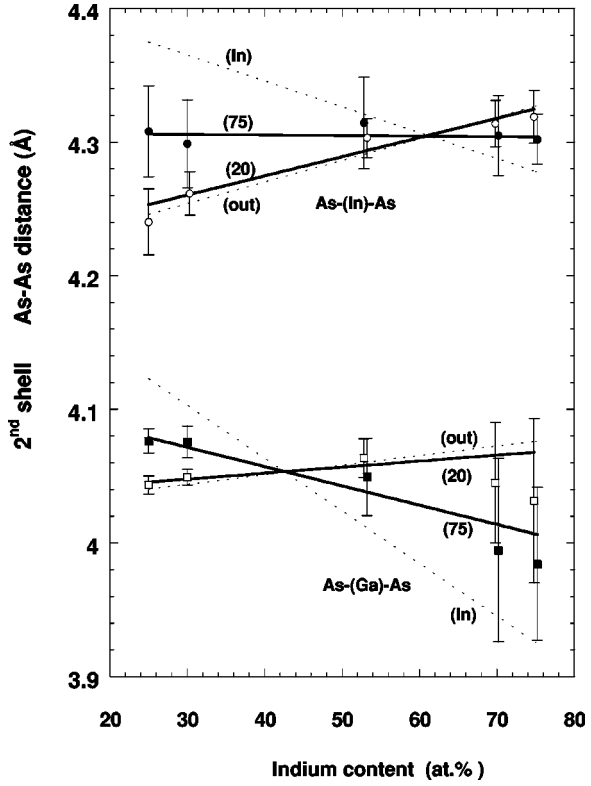

FIG. 7. As-(cation)-As second shell distances versus In atomic fraction: squares refer to $r^{2nd}_{\text{As-(Ga)-As}}$, circles to $r^{2nd}_{\text{As-(In)-As}}$. Open and solid symbols and dashed lines are coherent with those used in Fig. 6.

is the angle between the beam polarization vector and $\vec{r}$. Therefore the single atom contribution to the total signal can be enhanced aligning the polarization vector to its $\vec{r}$. For the same reason the contributions of the two subsets are dependent on the polarization orientation. When the polarization is aligned to the sample normal, the dominant contribution comes from the *out* subsets, whereas the signal from the atoms of the *in* subsets is largely suppressed. The vice versa happens when the polarization vector is parallel to sample surface.

A complete separation of the subset signals can be achieved only in the case that 90° angles are formed between the bond vectors of the two subsets. Moreover, experimental setup constraints do not permit to align the polarization exactly parallel and orthogonal to the [001] growth directions. Therefore a residual mixing effect of the subset signals will be always present and a further data analysis turns out necessary in order to obtain the subset distances.

We assume that each interatomic distance r obtained by the fit can be approximated by a weighted average of its subset values $r^{(in)}$ and $r^{(out)}$:

$$r = w^{(in)} r^{(in)} + w^{(out)} r^{(out)} \tag{1}$$

where $w^{(in)}$ and $w^{(out)}$ are the weights relative of the subset components in the XAFS signal (with normalization condition $w^{(in)}+w^{(out)}=1$). A more detailed justification of this approximation is given in Appendix.

The values of $w^{(in)}$ and $w^{(out)}$ have been calculated summing the contributions over homologous atoms of each subset. For the second shell it results that

$$w^{in}_{2nd}(\xi) = \sin^2(\xi)/2, \quad w^{out}_{2nd}(\xi) = 1 - \sin^2(\xi)/2, \tag{2}$$

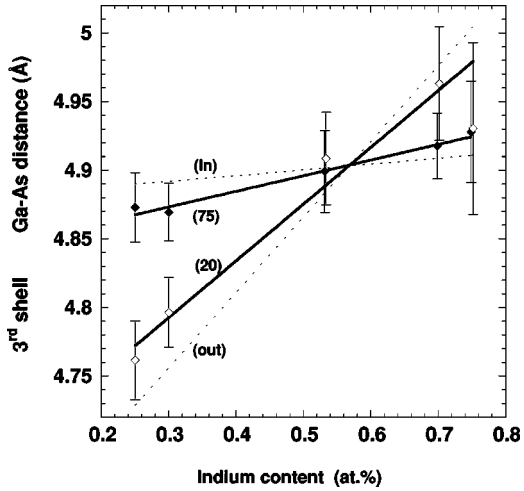

FIG. 8. Ga-As third shell distances versus In atomic fraction. Open and solid symbols and dashed lines are coherent with those used in Fig. 6.

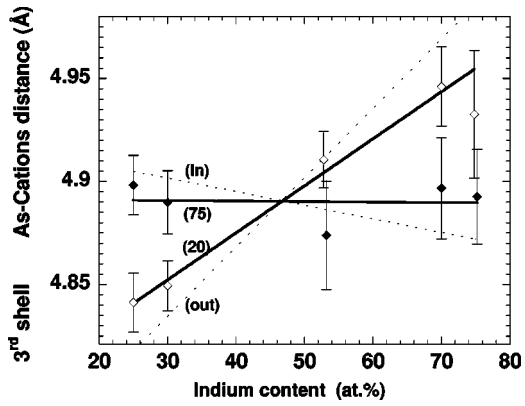

FIG. 9. As-cations third shell distances versus In atomic fraction. Open and solid symbols and dashed lines are coherent with those used in Fig. 6.

where ξ is the angle between the polarization vector and the normal to the sample surface. For the third shell it turns out to be

$$w_{3rd}^{in}=\frac{6-4\cos(2\xi)}{11}, \quad w_{3rd}^{out}=\frac{5+4\cos(2\xi)}{11}. \tag{3}$$

Having collected our measurements with two different polarizations ($\xi=75°$ and $\xi=20°$), Eq. (1) becomes actually a system with two equations and two variables. Inserting in Eqs. (2) and (3) the values of the polarization angles ξ the solution of the system can be written in matrix form as

$$\begin{pmatrix} r_{2nd}^{(in)} \\ r_{2nd}^{(out)} \end{pmatrix}=\begin{pmatrix} 2.308 & -1.308 \\ -0.143 & 1.143 \end{pmatrix}\begin{pmatrix} r_{2nd}(75) \\ r_{2nd}(20) \end{pmatrix}, \tag{4}$$

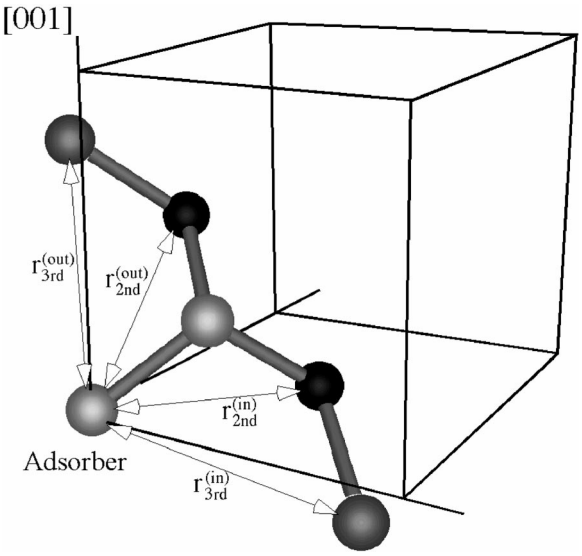

FIG. 10. Schematic representation of the nonequivalent atomic sites in the zincblende structure subject to a tetragonal strain. In second and third shells we distinguish the two subsets of nonequivalent sites by the indexes *in* and *out*.

TABLE III. Intercept and slope of the straight lines $\Delta r=s+\Delta s^*(x-0.53)$ describing the dependence on the In atomic fraction of the splittings [Eqs. (6) and (7)] of distance in second and third shell introduced by the epitaxial strain.

	s (Å)	Δs (Å)
$\Delta r_{2nd}^{\text{Ga-Ga}}$	-0.01 ± 0.02	0.31 ± 0.12
$\Delta r_{2nd}^{\text{Ga-In}}$	-0.01 ± 0.02	0.30 ± 0.09
$\Delta r_{2nd}^{\text{As-(Ga)-As}}$	-0.01 ± 0.03	0.36 ± 0.18
$\Delta r_{2nd}^{\text{As-(In)-As}}$	0.02 ± 0.03	0.46 ± 0.21
Weighted mean	-0.01 ± 0.01	0.33 ± 0.06
Model	0	0.286
$\Delta r_{3rd}^{\text{Ga-As}}$	-0.02 ± 0.03	0.51 ± 0.17
$\Delta r_{3rd}^{\text{As-(Ga/In)}}$	0.02 ± 0.02	0.40 ± 0.09
Weighted mean	0.01 ± 0.02	0.42 ± 0.08
Model	0	0.49

$$\begin{pmatrix} r_{3rd}^{(in)} \\ r_{3rd}^{(out)} \end{pmatrix}=\begin{pmatrix} 1.236 & -0.236 \\ -0.450 & 1.450 \end{pmatrix}\begin{pmatrix} r_{3rd}(75) \\ r_{3rd}(20) \end{pmatrix} \tag{5}$$

for the second and third shell, respectively. This procedure of data reduction allows to separate the mixing of the signals and determine the values of $r_{2nd}^{(in)}$, $r_{2nd}^{(out)}$, $r_{3rd}^{(in)}$, and $r_{3rd}^{(out)}$. Their dependence on the concentration was determined with a linear fit, shown in Figs. 6–9 as thin dashed lines. It clearly appears that the split of the *in* and *out* data fit is larger than the split of the experimental data.

In Table III we have reported the coefficients of the linear fit—as a function of x—of the distance *splits*:

$$\Delta r_{2nd}\equiv r_{2nd}^{(out)}-r_{2nd}^{(in)}=s_{2nd}+\Delta s_{2nd}(x-0.53), \tag{6}$$

$$\Delta r_{3rd}\equiv r_{3rd}^{(out)}-r_{3rd}^{(in)}=s_{3nd}+\Delta s_{3nd}(x-0.53). \tag{7}$$

The parameter s represents the value of the split in absence of strain and Δs is the slope of the linear fit. As expected, the values of s for both the second and the third shells are null within the error bar, indicating the absence of systematic errors due to the different polarization. Moreover, it is worth noting that the second shell split slopes are the same, within the error bar, with a weighted mean value equal to 0.33 ± 0.06 Å. Also the two third shell split slopes are very close with a mean value of 0.42 ± 0.08 Å.

VI. EFFECT OF STRAIN ON INTERATOMIC DISTANCES

A model for the calculation of the interatomic distance variation in a strained lattice has already been developed and has succesfully explained the XAFS results on IV and III-V alloy epitaxial films.[8–11] The underlying assumption of the proposed formalisms is that every vector $\vec{r}$ connecting two lattice sites transforms according to the macroscopic strain matrix $\overline{\overline{\varepsilon}}$ independently of the bond nature, its local environment, and alloying disorder effects. In this work we subject the above assumption to a more stringent test by predicting the strain effects up to the third coordination shell and comparing them to the experimental data presented in Sec. III.

The variation of the distance $\vec{r}$, induced by strain, can be written as

$$\delta r = |(\overline{\overline{I}} + \overline{\overline{\varepsilon}}) \cdot \vec{r}| - |\vec{r}|, \tag{8}$$

where $\overline{\overline{I}}$ is the identity matrix. Taking only the linear term of the series expansion in $\overline{\overline{\varepsilon}}$, it turns out to be

$$\delta r \simeq \frac{\vec{r}_{VC} \cdot \overline{\overline{\varepsilon}} \vec{r}_{VC}}{|\vec{r}_{VC}|}. \tag{9}$$

where $\vec{r}$ is approximated by the corresponding vector in the virtual crystal model.

In the case of tetragonal distortion it is straightforward to obtain the variation δr. The strain matrix is diagonal with the elements $\varepsilon_{xx} = \varepsilon_{yy} = \varepsilon_{\parallel}$, $\varepsilon_{zz} = \varepsilon_{\perp}$, related by the Poisson equation $\varepsilon_{\perp} = -\gamma \varepsilon_{\parallel}$, where γ is a combination of elastic constants, $\gamma = 2C_{12}/C_{11}$.[23] Then the distance variation of the second and third shells results to be, respectively,

$$\begin{pmatrix} \delta r_{2nd}^{(out)} \\ \\ \delta r_{2nd}^{(in)} \end{pmatrix} = \frac{a\epsilon_{\parallel}}{2\sqrt{2}} \begin{pmatrix} \gamma - 1 \\ \\ 2 \end{pmatrix}, \tag{10}$$

$$\begin{pmatrix} \delta r_{3rd}^{(out)} \\ \\ \delta r_{3rd}^{(in)} \end{pmatrix} = \frac{a\epsilon_{\parallel}}{4\sqrt{11}} \begin{pmatrix} 2 - 9\gamma \\ \\ 10 - \gamma \end{pmatrix}, \tag{11}$$

where a is the lattice parameter. The splits between the two distance subsets are then given for the second shell by: $\Delta r_{2nd} = \delta r_{2nd}^{(out)} - \delta r_{2nd}^{(in)}$ and $\Delta r_{3rd} = \delta r_{3rd}^{(out)} - \delta r_{3rd}^{(in)}$. By Eq. (10) one can obtain for the second shell

$$\Delta r_{2nd}^{th} = \delta r_{2nd}^{(out)} - \delta r_{2nd}^{(in)} = 0.286(x - 0.53) \quad \text{Å}. \tag{12}$$

and the third shell by

$$\Delta r_{3rd}^{th} = \delta r_{3rd}^{(out)} - \delta r_{3rd}^{(in)} = 0.49(x - 0.53) \quad \text{Å}, \tag{13}$$

The experimental values of the splits reported in Table III, show an excellent agreement with the prediction of the model for both the second and the third shell.

VII. DISCUSSION

The previous results suggest a discussion on the microscopic elastic constants. The main result of this study is the possibility of describing the effect of strain at a local level independently of the nature of the bond. Indeed, the split slopes of all the second- and third-shell distances are the same coherently with the predictions of our model that applies the macroscopic strain matrix to a local scale.

This point could appear quite surprising since the valence force field potential (VFF), commonly used to calculate the interatomic distances of covalent semiconductor alloys, predicts quite different local elastic constants depending on the different kind of bonds. For example, the bond bending elastic constant β used in the Kirkwood model[24] are $\beta(\text{InAs}) = 5.75$ and $\beta(\text{GaAs}) = 9.26$ N/m for the triangles As-(In)-As and As-(Ga)-As, respectively.[5] Nevertheless this large difference in the elastic constants does not seem to originate two different values of the splits $\Delta r_{2nd}^{\text{As-(Ga)-As}}$ and $\Delta r_{2nd}^{\text{As-(In)-As}}$ (see Table III). An analogous observation was already reported relatively to the effect of the strain on the first-shell distances.[25]

This behavior is confirmed by considering the Cai and Thorpe calculations.[5] In this work, the interatomic distances of the $In_xGa_{1-x}As$ unstrained system are calculated with two different approaches. The first uses a single *average* set of local elastic constants for In-As and Ga-As bonds (analytical method). The second approach numerically evaluates the interatomic distances using different local elastic constant in the effective medium approximation (EMA). The best agreement with the experimental data[1] has been obtained by the first *average* approach. On the contrary, the EMA calculation of Cai and Thorpe predicts a deviation from the linear dependence on composition of the lattice constant of the In-As first shell distance that has not been measured.[1] Indeed a negative bowing parameter for the average NN distance in $In_xGa_{1-x}As$ alloy is reported by Cai and Thorpe.[5] The bowing, i.e., the coefficient of the second-order term in the mean interatomic distance as a function of the composition, is reported to be equal to -0.0116 Å. This should corresponds to a maximum deviation of -0.0067 Å in the mean lattice parameter. Our cross check of RBS and XRD brings to a maximum deviation inside ± 0.002 Å confirming the data reported by Mikkelsen and Boyce[1] that show a Vegard's law behavior for the lattice parameter of $In_xGa_{1-x}As$.

The present results and the reported discrepancies with the EMA calculations by Cai and Thorpe suggest that the macroscopic elastic constants describe the local behavior of the interatomic distances better than the local constants of the VFF model. The latter are extracted from the elastic properties of the bonds when a single atom is embedded in a binary compound and cannot probably be directly transferred to the alloy. A strong coupling of the local elastic constants with the effective medium can explain the reported results. In other words it seems that the local elastic constants for different kinds of bonds are close to each other more than that predicted by the VFF model.

VIII. CONCLUSIONS

Polarization-dependent XAFS measurements have shown that the second- and third-shell interatomic distances of $In_xGa_{1-x}As$ epitaxial layers under tetragonal distortion split into two subset distributions. The experimental results are reproduced very well by a model that applies the macroscopic strain tensor to the interatomic distances independently of the atoms and bonds involved. This fact suggests that the matrix in which each single bond or bond angle is actually embedded introduces a smoothing of the local fluctuations of the lattice structure response to an external strain field.

ACKNOWLEDGMENT

XAFS measurements were performed at European Synchrotron Radiation Facility (ESRF) in Grenoble (France) within the public user program.

APPENDIX

In Sec. V we have introduced the hypothesis that the XAFS signal of a bimodal distribution of interatomic distances could be reproduced with good accuracy with the signal of a single gaussian component, provided that the two distances of the original distribution are sufficiently close to each other. The purpose of this assumption was twofold: reducing the number of free parameters used in the fit, and introducing a scheme for a quantitative interpretation of polarization-dependent measurements of the interatomic distances. However, a detailed justification of our assumptions seems necessary in order to corroborate the results of the analysis. To this purpose we define

$$\chi_R(k)=A(k)\sin[2kR+\phi(k)], \tag{A1}$$

which represents the general form of a XAFS signal for a given photoabsorber-scatterer distance R. In case of a bimodal distribution with peaks centered in R_a and R_b the signal is given by

$$\langle\chi(k)\rangle=w_a\chi_{R_a}(k)+w_b\chi_{R_b}(k), \tag{A2}$$

where w_a and w_b are the relative weights of the two components ($w_a+w_b=1$).

We want to show that the signal $\langle\chi(k)\rangle$ is well approximated by a signal of the form $\chi_R(k)$ [Eq. (A1)], and that the best fit of $\langle\chi(k)\rangle$ is obtained by a signal $\chi_{R_{fit}}(k)$, where R_{fit} is given with a good approximation by the weighted average of the distances ($R_{fit}\approx w_aR_a+w_bR_b$). By defining

$$R^*=w_aR_a+w_bR_b \quad \Delta R=R_a-R_b\,, \tag{A3}$$

it is possible to write the signal for the bimodal distribution as follows:

$$\langle\chi(k)\rangle=A(k)\{w_a\,\sin[2k(R^*+w_b\Delta R)+\phi(k)] + w_b\,\sin[2k(R^*-w_a\Delta R)+\phi(k)]\}. \tag{A4}$$

Using standard trigonometrical transformations, the previous expression can be set in the form

$$\langle\chi(k)\rangle=A(k)\{g_w(2k\Delta R)\sin[2kR^*+\phi(k)] + f_w(2k\Delta R)\cos[2kR^*+\phi(k)]\}, \tag{A5}$$

where

$$f_w(x)=w_a\,\sin(w_bx)-w_b\,\sin(w_ax) \tag{A6}$$

$$g_w(x)=w_a\,\cos(w_bx)+w_b\,\cos(w_ax). \tag{A7}$$

The index w reminds that these functions depend on the statistical weight of the two components of the signal. We notice that $f_w(x)$ and $g_w(x)$ are, respectively, odd and even functions of x. It is also important to observe that the first term of the series expansion of $f_w(x)$ is cubic in the variable x; this fact derives from the definition of the point R^*, Eq. (A3). Any different value of R^* would have led to the definition of a function $f_w(x)$ with a linear term in x. On the contrary the expansion of $g_w(x)$, contains also the zero-order term [$g_w(0)=1$].

We have analyzed the function $g_w(2k\Delta R)$ and $f_w(2k\Delta R)$ in order to evaluate the approximation of neglecting the second term of Eq. (A5) and to demonstrate the possibility of absorbing the factor $g_w(2k\Delta R)$ in front of $\sin[2kR^*+\phi(k)]$ by a redefinition of the Debye-Waller coefficient in the amplitude $A(k)$.

The cubic dependence of $f_w(2k\Delta R)$ on the product $k\Delta R$ suggests that the approximation made by neglecting the contribution to the signal proportional to $\cos[2kR^*+\phi(k)]$ may become critical at large values of the separation ΔR between the two components present in the signal, and at high values of k. Furthermore, the approximation depends also on the value of the weight $w_a(w_b)$. For instance, in the case of equal weight of the two components ($w_a=w_b=0.5$) $f_w(2k\Delta R)\equiv 0$.

Therefore, it is important to consider in detail the case of the weights used in the second and third shell analysis. In the case of the second shell distances the weights considered were $w_a=0.466$ ($w_b=0.534$) for the measurements at $\xi=20$ deg and $w_a=0.059$ ($w_b=0.941$) for $\xi=75$. It is possible to show that in both cases the function $|f_w(2k\Delta R)|$ does not exceed 0.04 in the domain $(k,\Delta R)\in[0,9]\times[0.0,0.10]$ ($\text{Å}^{-1}\times\text{Å}$); this upper limit becomes larger (~ 0.10) only for separations $\Delta R=0.15$ Å. In other words, the contribution to the signal proportional to $\cos[2kR^*+\phi(k)]$ is few percent of the total signal, attaining, at most, values of the order of 10% in case of maximum distance separations (samples with the highest strain) at the end of the useful part of the spectra. In the case of the third shell distances the useful part of the spectra is limited to 8 Å^{-1} (see Figs. 2 and 3); analogous to what is done for the second shell, it is possible to show that the upper limit to $|f_w(2k\Delta R)|$ is 0.15 in the domain $(k,\Delta R)\in[0,8]\times[0.0,0.15]$ $\text{Å}^{-1}\times\text{Å}$ for any choice of the weight w_a. This value decreases to less than 0.05 for $\Delta R\leqslant 0.1$. Summarizing, we have shown that the signal proportional to $\cos[2kR^*+\phi(k)]$ is about one order of magnitude weaker than the signal proportional to $\sin[2kR^*+\phi(k)]$, and then well below the noise level in the experimental spectra so that it can be neglected.

As already mentioned, we have found that the k dependence of the factor $g_w(2k\Delta R)$ can be well approximated by a function of the type $\exp[-2k^2\Delta\sigma^2]$; the result is a correcting factor to the values of the Debye-Waller factors determined from the fits. We have established this approximation, the accuracy of which depends on the values of ΔR and w, by a numerical study. It was found that the two functions $g_w(2k\Delta R)$ and $\exp[-2k^2\Delta\sigma^2]$ are equal within better than 5% in the k range from 3 to 10 Å^-1; the correction to the Debye-Waller parameter is usually in the order of few 10^{-3} Å^2.

*Present address: Physikalisches Institut, Universität Würzburg, Am Hubland, 97074 Würzburg, Germany.

[1] J.C. Mikkelsen and J.B. Boyce, Phys. Rev. B **28**, 7130 (1983).
[2] A. Balzarotti, M.T. Czycyk, A. Kisiel, N. Motta, M. Podgorny, M. Zimnal-Starnawska, Phys. Rev. B **30**, 2295 (1984).
[3] J.L. Martins and A. Zunger, Phys. Rev. B **30**, 6217 (1984).
[4] Y. Cai and M.F. Thorpe, Phys. Rev. B **46**, 15 872 (1992).
[5] Y. Cai and M.F. Thorpe, Phys. Rev. B **46**, 15 879 (1992).

[6] Y. Kuwahara, H. Oyanagi, R. Shioda, Y. Takeda, H. Yamaguchi, and M. Aono, Jpn. J. Appl. Phys. **33**, 5631 (1994).
[7] M. Tabuchi, T. Kumamoto, and Y. Takeda, J. Appl. Phys. **77**, 143 (1995).
[8] J.C. Woicik, C.E. Bouldin, K.E. Miyano, and C.A. King, Phys. Rev. B **55**, 15386 (1997).
[9] J.C. Woicik, J.G. Pellegrino, B. Steiner, K.E. Miyano, S.B. Bonpadre, L.B. Sorensen, T.-L. Lee, and S. Khalid, Phys. Rev. Lett. **79**, 5026 (1997).
[10] F. Romanato, D. De Salvador, M. Berti, A. Drigo, M. Natali, M. Tormen, G. Rossetto, S. Pascarelli, F. Boscherini, C. Lamberti, and S. Mobilio, Phys. Rev. B **57**, 14 619 (1998).
[11] M. Tormen, D. De Salvador, M. Natali, A. Drigo, F. Romanato, G. Rossetto, F. Boscherini, and S. Mobilio, J. Appl. Phys. **86**, 2533 (1999).
[12] P.A. Lee, P.H. Citrin, P. Eisenberger, and B.M. Kincaid, Rev. Mod. Phys. **53**, 769 (1981).
[13] M. Servidori, F. Cembali, R. Fabbri, and A. Zani, J. Appl. Crystallogr. **25**, 46 (1992).
[14] For a description of the analysis technique see A. Armigliato, M. Servidori, F. Cembali, R. Fabbri, R. Rosa, F. Corticelli, D. Govoni, A.V. Drigo, M. Mazzer, F. Romanato, S. Frabboni, S.S. Iyer, and A. Guerrieri, Microsc. Microanal. Microstruct. **3**, 363 (1992).
[15] S. Pascarelli, F. Boscherini, F. D'Acapito, J. Hrdy, C. Meneghini, and S. Mobilio, J. Synchrotron Radiat. **3**, 147 (1996).
[16] S.I. Zabinsky, J.J. Rehr, A. Ankudinov, R.C. Albers, and M.J. Eller, Phys. Rev. B **52**, 2995 (1995).
[17] M. Newville, B. Ravel, D. Haskel, J.J. Rehr, E.A. Stern, and Y. Yacoby, Physica B **208&209**, 154 (1995).
[18] M. Newville, P. Livins, Y. Yacoby, J.J. Rehr, and E.A. Stern, Phys. Rev. B **47**, 14126 (1993).
[19] Error Reporting Recommendation: A Report of the Standards and Criteria Committee, July 26, 2000 of the International XAFS Society, available at http://ixs.csrri.iit.edu/IXS/subcommittee_reports/sc/err-rep.pdf
[20] C. Brouder, J. Phys.: Condens. Matter **2**, 701 (1990).
[21] E. Stern, Phys. Rev. B **48**, 9825 (1993).
[22] We use the factor $3\cos^2(\theta)$ to describe the polarization dependence of XAFS signal. This commomly used method is rigorously valid only in the single scattering plane wave approximation (see Ref. 20). The contribution of MS signals to our data analysis has already been discussed. The plane wave approximation is more adequate for atomic correlations at distances greater than the first shell.
[23] The value γ has been assumed equal to the average of its value in InAs (0.9) and GaAs (1.09), being the nonlinear dependence on composition x negligible.
[24] J.G. Kirkwood, J. Chem. Phys. **7**, 506 (1939).
[25] J.C. Woicik, Phys. Rev. B **7**, 6266 (1998).